PAPER

Check for updates

Impact dynamics of non-ferro liquid droplets under magnetic influence

Ghassan Hassan, [abc] Bekir Sami Yilbas, *[abc] Abdullah Al-Sharafi[abc] and Hussain Al-Qahtani[ab]

Impacting non-ferro liquid (water) droplets on a hydrophobic surface finds many applications in various sectors. Controlling droplet behavior on the impacting surface remains critically important in terms of affecting contact duration, spreading and contraction rates, and rebound height. Introducing an external magnetic influence on droplets considerably alters the impact characteristics. Consequently, the present study investigates the impacting of water droplets on hydrophobic surfaces with loosely dispersed low-surface-energy ferro particles. Since the interfacial force between the particles and water is large, a droplet picks up some ferroparticles, which are pinned on the droplet surface despite the presence of the magnetic field. The particles pinned on the droplet surface alter the droplet behavior at the impacted surface under the magnetic field. In order to assess the mechanism of how particles are picked up by the impacting droplet liquid, the particles are functionalized to reduce the surface energy. It is demonstrated that the functionalized particles are picked up by the water droplet; however, they are pinned at the droplet surface rather than being immersed into the droplet fluid. The interfacial force due to particles pinned on the droplet surface is higher than the magnetic force created under the magnetic field. This gives rise to lower contact time, droplet spreading, and rebound height. This is more pronounced at low Weber numbers.

Introduction

Impacting droplets have many industrial applications and some of which are related to surface cooling,[1] in biomedicine,[2] bioprinting,[3] surface cleaning[4] and similar. In impacting droplet studies, the combination of magnetic forces with surface hydrophobicity enables researchers to introduce new aspects for designing adaptive surfaces that could provide greater versatility for practical applications in diverse industries, from aerospace to biomedical devices. The droplet liquid possibly wets particles upon impact due to a positive spreading coefficient, which enables particles to suspend in the droplet fluid.[5] Ferroparticles can be magnetized while creating a magnetic force on the droplet surface and the size and number density of the ferroparticles can alter the magnitude of the magnetic force. In some cases, ferroparticles may cluster together within a droplet or around the droplet surface while leading to the formation of unique structures or patterns.[6] When a magnetic field is applied, the clustering of ferroparticles results in local and directional magnetic forces acting on the droplet. Hence,

the mobility of droplets on hydrophobic surfaces can be enhanced and controlled *via* the presence of ferroparticles under externally applied magnetics fields.[7] The control of droplet mobility can be fruitful in areas like microfluidics, environmental monitoring, energy storage, and surface cleaning. However, low surface energy particles cannot be wetted by a droplet fluid during impact. These particles cannot immerse into the droplet fluid but rather pin on the droplet surface. Hence, they can create a magnetic influence on droplet mobility as an external magnetic field is applied.

As a droplet contacts a hydrophobic surface, the low contact angle causes less droplet adhesion while enhancing available kinetic energy of the droplet on the hydrophobic surface. In general, the dynamics of the impact are governed by the spreading, retraction and rebounding, or coalescence of the liquid. However, the factors affecting the impact dynamics include surface roughness and texture, free energy, impact height, liquid viscosity, and liquid mass. The surface texture and roughness contribute to repellency of the droplet by trapping air in the texture sites while creating pressure force between the liquid and the surface.[8,9] The droplet viscosity gives rise to a shear region at the droplet bottom and causing a shear force adverting droplet expansion while contributing to kinetic energy loss. Moreover, the spreading behavior of droplets on hydrophobic surfaces is influenced by force ratios as described by the droplet Weber number (We) and Reynolds number (Re).

ᵃMechanical Engineering Department, King Fahd University of Petroleum and Minerals (KFUPM), Dhahran 31261, Saudi Arabia. E-mail: bsyilbas@kfupm.edu.sa; Tel: +966 3 860 4481

ᵇInterdisciplinary Research Center for Sustainable Energy Systems (IRC-SES), King Fahd University of Petroleum and Minerals (KFUPM), Dhahran 31261, Saudi Arabia

ᶜK.A.CARE Energy Research & Innovation Center, Dhahran 31261, Saudi Arabia

At high droplet Reynold numbers, the viscous dissipation at the droplet-impacted surface becomes high and the frictional work done increases during droplet expansion and retraction. However, a critical Weber number (We), which represents the relative importance of inertial forces to surface tension forces, is one of the key parameters in assessing a droplet's spreading behavior. The physical correlation between surface roughness, surface energy, and droplet velocity influences the dynamic behavior such that droplet coalescence, formation of satellite droplets or splashing can result due to a thin film formed at the surface before undergoing significant recoil or splashing.[10] At high Weber numbers, the impact velocity remains high, resulting in increased spreading upon impact.[11] For hydrophobic surfaces, there is a limit to the maximum liquid spread because of a strong surface repulsion force that counteracts the droplet's inertia. Attempts to predict the maximum spread factor using scale laws[12] or empirical formulation[13] may not result in very appropriate estimation for applications related to ferrofluid droplet impact. In addition, momentum balance[14] or energy equations based on early formulations[15] for assessing the spread factor have limitations for a droplet fluid mixed with small particles. The formulation of the spread factor incorporating combined power laws covering capillary and viscous regimes provides relatively accurate predictions of impact characteristics of droplet fluid without particles.[16] Moreover, improving surface hydrophobicity, through surface coatings, significantly alters the droplet dynamics, allowing fast rebound rates on the surface.[17] This remains crucial for self-cleaning applications, where surface contaminants are removed by the droplet fluid *via* spreading and rolling motion after impact.

The magnitude of a magnetic force, created at the interface of particles and droplet fluid, can remain high[18] while affecting the dynamic behavior of the onset of droplet impact, despite the fact that ferroparticles are loosely spread over impacting surface. In this case, the loose particles act like a third body at the surface altering contact angle, surface tension, and interfacial surface friction, and increasing droplet mass *via* surface attachments.[19] Depending on the force created, due to the magnetic effect, on the loose particles, some particles are magnetically attached and remain part of the surface while others may still attach to the droplet surface upon impact. The balance between the interfacial force between droplet fluid and the magnetic force defines the loose particle status on the impacted surface. Hence, an external applied magnetic field could potentially induce a variation in the texture or the wetting properties by pulling or pushing the magnetic loose particles while leading to a transient behavior in the liquid contact angle.[20] At low magnetic field strengths, this effect on the droplet spreading may become subtle; however, at high magnetic fields, the modified surface can significantly influence the droplet dynamics, potentially allowing for new paths of spreading and recoiling.[21] This becomes especially interesting in applications where the droplet dynamics may need to be precisely controlled, such as in microfluidic applications or self-cleaning of surfaces, where the ability to manipulate droplets *via* magnetic fields provides a leverage for controlling droplet motion over hydrophobic surfaces. Moreover, in self-cleaning

and anti-icing applications, the integration of ferroparticles with hydrophobic surfaces can be considered to change the surface hydrophobicity depending on the desired or expected outcome. Applying external magnetic fields can assist in ensuring that droplets maintain a spherical shape for efficient contaminant cleaning operation by preventing the formation of surface icing under freezing conditions.[22]

Although ferrofluid droplet impact on hydrophobic surfaces and droplet behavior have been investigated and explored previously,[5,18,19,21] magnetic control of impacting non-ferro liquid droplets on hydrophobic surfaces in the presence of hydrophobized ferroparticles has been less studied. However, hydrophobized loose ferroparticle interaction with non-ferro liquid, like water, droplets under a magnetic field can alter the droplet spreading factor, restitution coefficient, contact duration, and rebound height after impact. This is because introducing hydrophobized loose ferroparticles at a hydrophobic surface adds a layer of complexity while influencing non-ferro droplet dynamics because of modification of surface topology and forces created on the droplet. Manipulation of non-ferro liquid droplets by an external magnetic force extends the practical applications of droplets, particularly in biomedicine *via* manipulation of water droplets by a magnetic field. Moreover, the magnetic tunability of droplets enables precise spatiotemporal control over their movement and deformation, making them especially attractive for applications where non-contact manipulation is vital, such as in sterile biomedical environments or closed microfluidic systems,[23] and accurate deposition of contactless non-ferro droplets with minimum waste in high-tech printing and coating technologies. On the other hand, droplet fluid spreading over ferroparticles can be prevented by hydrophobizing the particles; in which case, the hydrophobized ferroparticles can pin and attach to the droplet outer surface (droplet boundary) upon impact, unlike the case observed for non-hydrophobized ferroparticles.[24] Consequently, the present study investigates the characteristics of droplets impacting on sparsely distributed loose ferroparticles, placed on a hydrophobic surface, under the influence of a magnetic field. The droplet spreading and contraction rates and droplet rebound height are measured experimentally and estimated from analytical formulations. The study is extended to include examining the influence of magnetic force on impacting droplet characteristics as the ferroparticles are hydrophobized lowering the surface energy to result in a negative spreading coefficient of droplet fluid over the ferroparticle surface. In addition, the experiments are repeated for surfaces without ferroparticles to analyze and demonstrate the influence of a magnetic field on the dynamics of impacted droplets.

Experimental

Glass sheets were used, the surface of which was hydrophobized *via* deposition of nano-size synthesized silica nanoparticles by using a dip coater (Biolin Scientific). The immersion and withdrawal speeds were kept the same at 0.005 mm s^{-1} during the dip-coating process. The solution for surface hydrophobizing was prepared according to the mixture used in a previous

study,[25] *i.e.* tetraethyl orthosilicate (TEOS), iso-butyltrimethoxysilane (OTES), ethanol, and ammonium hydroxide solution was prepared accordingly. A Kyowa model DM 501 goniometer was used for assessing the droplet contact angle and hysteresis. It is worth mentioning that measurements of contact angle and contact angle hysteresis were repeated for all samples to ensure uniform and same wetting state of the hydrophobized surfaces. The ferroparticles (Fe_3O_4, Sigma Aldrich) with ≤50 nm sizes were loosely distributed over the hydrophobized surface while ensuring uniform distribution of the particles. In addition, separately, ferroparticles were functionalized with TEOS solution to reduce the surface free energy, and the resulting hydrophobized particles were used in the second cycle of the experiments, in which the same procedures as for the first cycle (non-hydrophobized ferroparticles case) were adopted. It is worth mentioning that during the functionalizing process, some ferroparticles clustered forming globule-like structures with micrometer sizes. A magnet (NdFeB, K&J Magnetics Inc., USA) was utilized in the experimental setup. A numerical frame was incorporated for precise water droplet impacting at the particle-distributed hydrophobic surface. Fig. 1 gives a sketch of the experimental arrangements. A camera operating at high speed (speed sense 9040) was employed for real-time capturing of droplet motion during and after the impact. A program was accommodated quantifying the recorded camera data. The data were captured at a rate of 5000 frames per second (fps) and the images had 1280 × 800 pixels with a pixel size of 14 μm × 14 μm. The uncertainty analysis was carried out using the following relation:[26]

$$\sigma_u = \sqrt{\int_{x_o}^{x_n}(x-\beta_e)^2 p(x)\mathrm{d}x}$$ (1)

where β_e is the average droplet velocity during impact on the sample surface, n is the number of velocity repeats, and $p(x)$ is the velocity data distribution function in Gaussian form. The bias uncertainty was assessed *via* evaluating the small peaks in the distribution function. The uncertainty was estimated as 2.8%.

Fig. 2a and b show the spread of as-received and functionalized ferroparticles on the water surface and their immersion
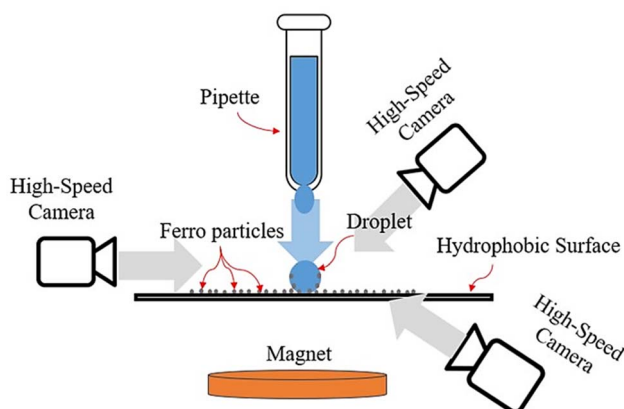
states at different times while Fig. 2c and d depict the attachment of functionalized ferroparticles on a water droplet surface. It is evident that the functionalized ferroparticles do not immerse into the water but rather float at the surface due to low surface free energy, unlike the as-received ferroparticles on the water surface, which immerse into the water over time. Fig. 2c depicts the attachment of ferroparticles on a droplet surface. This is because the functionalized silica particle surface possesses a hydrophobic wetting state; hence, the functionalized silica particles remain attached to the droplet surface rather than piercing the surface and immersing into the droplet fluid, as observed from Fig. 2b. It is worth mentioning that the spreading parameter (S) can be formulated *via* surface free energy of ferroparticles (γ_{SA}), interfacial tension across water and ferroparticle surface (γ_{SL}), and the surface tension of water (γ_{LA}) through the relation: $S = \gamma_{SA} - \gamma_{SL} - \gamma_{LA}$. In this case, the surface free energy of ferroparticles (γ_{SA}) is estimated to be 1.145×10^3 mJ m^{-2}, the interfacial tension (γ_{SL}) is ∼ 0.125×10^3 mJ m^{-2}, surface tension is ∼ 0.073 N m^{-1}, and the spreading factor (S) becomes about 948×10^3 mJ m^{-2}; as a result, water droplets wet the untreated ferroparticles.[27,28] However, the surface free energy of functionalized particles is ∼ 38.2 mJ m^{-2}, which is significantly smaller than that of the unfunctionalized ferroparticles while giving rise to a negative spreading factor.[29] Fig. 3a and b show AFM data of the hydrophobized surface and while Fig. 3c demonstrates an SEM image of same surface.[30] The topology consists of clustered particles of almost 30 nm in size and the cluster height varies between 25 nm and 130 nm forming the texture. The mean roughness of the surface (R_a) is almost 80 nm, and sub-micron cavities form in between clustered particles while covering 27% of the synthesized surface area. The hydrophobic state of the synthesized sample surfaces was evaluated by a goniometer and the water droplet contact angle is ∼150° ± 2°, with a hysteresis of 2° ± 1°. Moreover, as the droplet impacts on the non-functionalized ferroparticles on the hydrophobic surface, some ferroparticles are picked up by the droplet fluid, which may slightly change the surface tension. Hence, sets of tests were carried out to measure the particle concentration in the droplet fluid after the impact and the percentage weight gain of the droplet fluid was estimated as ∼ 0.17%. It is worth mentioning that droplet weight gain was measured by a sensitive microbalance (Borealis BA-T/BA Series). In addition, the contact angle measurements were repeated for droplets with functionalized particles on the surface, and the change is found to be about ±1° due to ferroparticles pinning on the droplet surface. SEM images of the as-received and synthesized ferroparticles are shown in Fig. 3d and e. The functionalized surface possesses a whisker-like texture emerging from the ferroparticle surface (Fig. 3e). On the other hand, an applied magnetic field may influence the contact angle for the case of functionalized ferroparticles pinned on the droplet surface after impact. This condition was tested experimentally, and the contact angle change is found to be negligible (∼1%) because of the non-mixing of particles with the droplet fluid and the magnet location, which is away from the surface impacted (70 mm). However, a ferrofluid droplet in the stand-off position (onset of
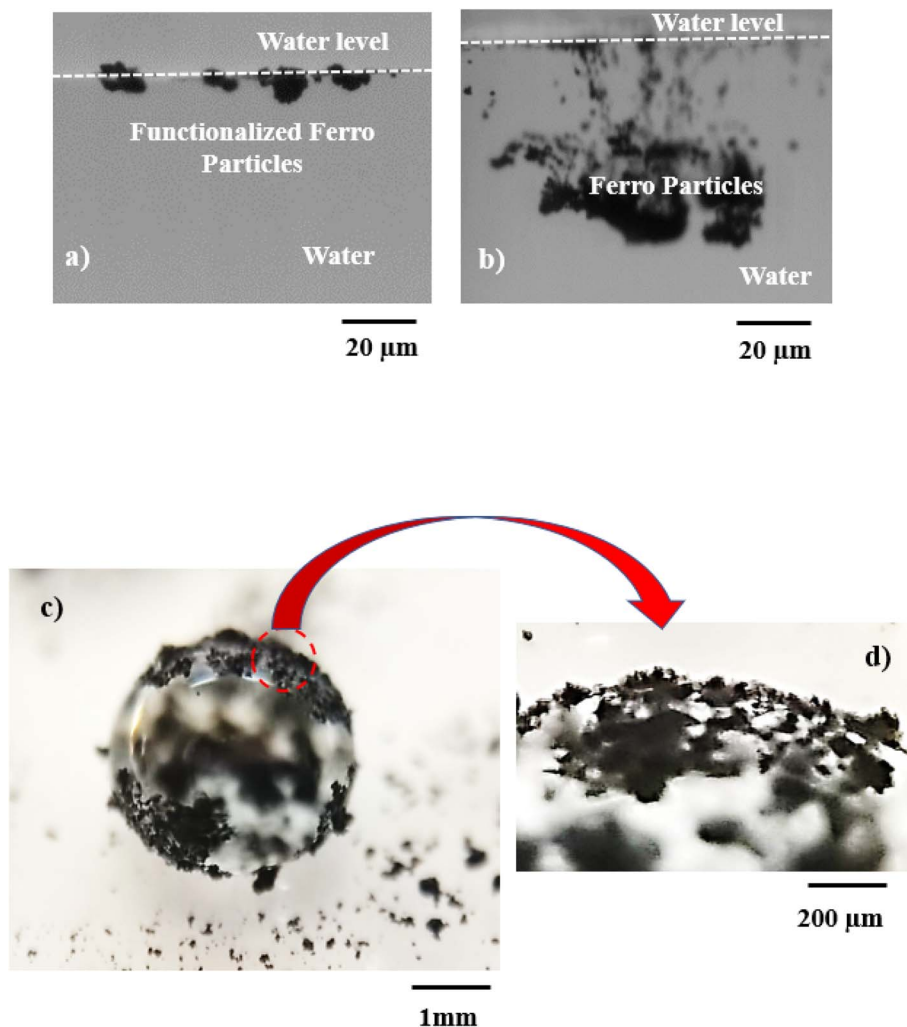

Fig. 1 A schematic view of the experimental setup.

Fig. 2 (a) Functionalized ferroparticles floating on the water surface due to low surface free energy. (b) Immersion of as-received ferroparticles into water due to high surface free energy. (c) An optical image of functionalized ferroparticles attaching to the droplet surface. (d) An optical image showing a close-up view of functionalized ferroparticles attaching to the droplet surface.

exiting from the pipette) is influenced significantly by the magnetic field and its trajectory changes slightly prior to impact.[31] However, in the current study, the water droplet impacts onto the hydrophobic surface with loosely dispersed ferroparticles for the cases of as-received and functionalized ferroparticles. Hence, a magnetic influence on the falling droplet prior to impact is not observed experimentally because there are no functionalized ferroparticles on the droplet surface during the free-fall period.

Results and discussion

The dynamic properties of a droplet that impacts on a hydrophobic surface having loosely placed ferroparticles are investigated under the circumstances of with and without an applied magnetic field. The conditions for particles picked up by the droplet are explored *via* functionalizing the particles to reduce their surface energy. The force analysis and dynamic behavior of the droplet after impact are analyzed and discussed accordingly.

Force analysis

A droplet impacting on a hydrophobic surface with loosely located non-functionalized ferroparticles is considered and the behaviors of droplet and particles are analyzed experimentally and analytically. The wetting of water (droplet liquid) over as-received (non-functionalized) ferroparticles remains critical for particles to be picked by the droplet fluid while ensuring adequate wetting and coverage of particles by fluid. The spreading parameter (S) of the droplet fluid must maintain a value exceeding zero (positive value):

$$S = \gamma_p - \gamma - \gamma_{p-w} \tag{2}$$

where γ_p is the surface free energy of particles (1.145×10^3 mJ m^{-2}),[32] γ is the fluid surface tension with a value of 0.0738 N m^{-1}, and γ_{p-w} is the interfacial tension with a value of 0.125×10^3 mJ m^{-2}.[33] The spreading coefficient (eqn (2)) becomes positive and is around 947 mJ m^{-2}. Therefore, the droplet liquid wets the non-functionalized ferroparticles. To maintain the ferroparticles in the droplet fluid, the capillary force (F_γ) and
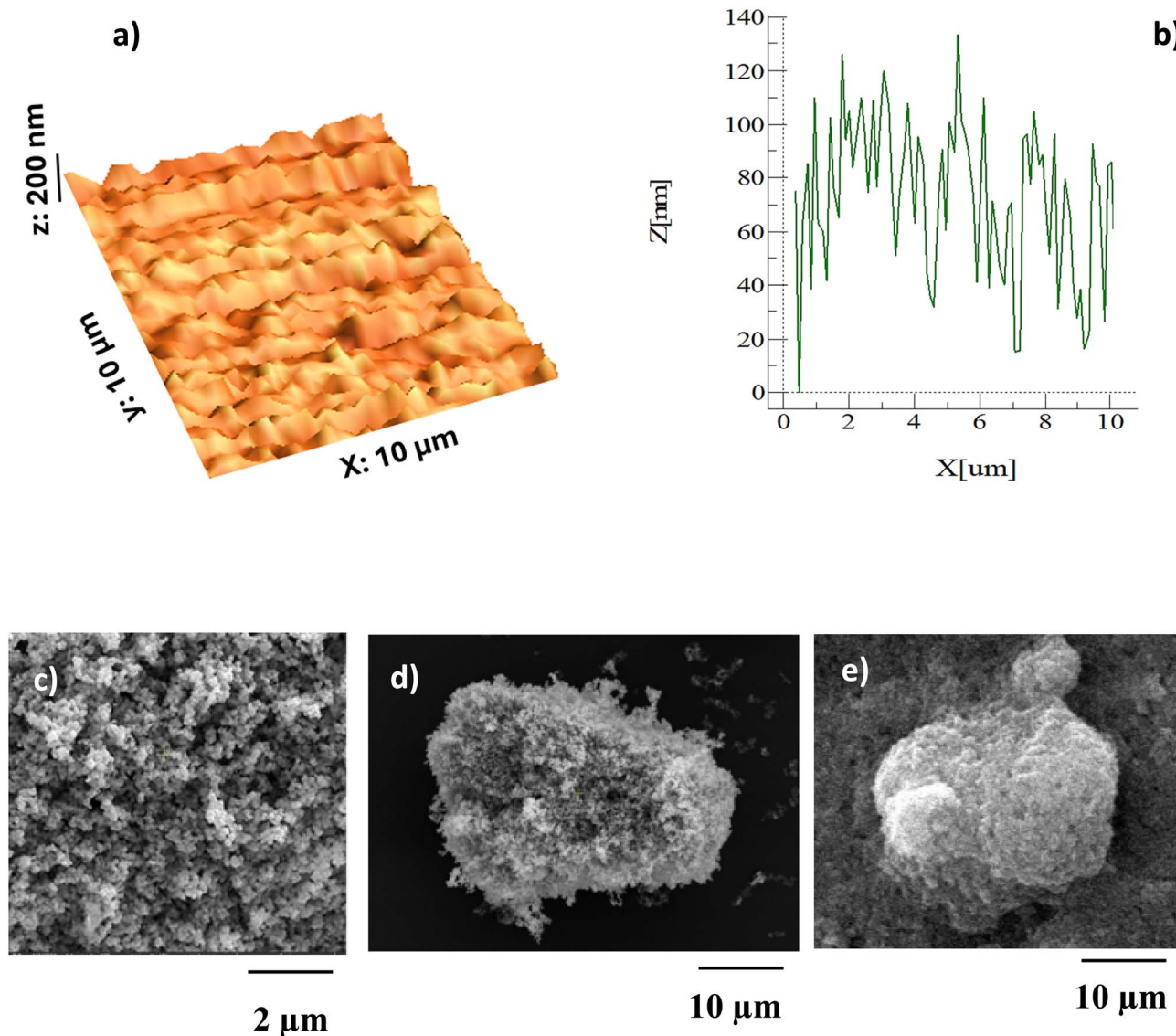
Fig. 3 (a) AFM topology of the hydrophobic surface.[5,30] Synthesized surfaces have various topologies. (b) An AFM line scan of the hydrophobic surface. The surface topology consists of hill-like structures with a maximum peak height of about 132 nm.[5,30] (c) An SEM micrograph of the hydrophobic surface.[5,30] The clustering of nanosized (30 nm) synthesized silica particles is evident while forming hill-like structures. (d) An SEM micrograph of synthesized ferroparticles[5,30] and (e) an SEM micrograph of an as-received ferroparticle.

buoyancy force acting on particles must be of similar order to the gravitation force. The capillary force is formulated in the context of an earlier study,[34] *i.e.*:

$$F_\gamma = 6^{\frac{1}{3}} \, \pi^{\frac{2}{3}} \, \gamma_{p-w} \left[\frac{m_p}{\rho_c} \right]^{\frac{1}{3}} \tag{3}$$

Here, m_p is particle mass. Due to the magnetic effect, particles aggregate within the liquid. The mass of the loose particles is estimated to be $\sim 5.5 \times 10^{-11}$ kg. Since tension at the liquid–particle interface is 0.125 N m^{-1}, the force (F_γ) computed at the interface from eqn (3) is $\sim 1.56 \times 10^{-4}$ N. Buoyancy force (F_{Bp}) for particles inside the droplet is 3.21×10^{-7} N ($F_{Bp} = \gamma_{sp} \, \forall_p$, where $\forall_p$ is the volume of the particles while γ_{sp} is the specific weight of liquid), which becomes smaller than the interfacial force. The weight of particles inside the droplet is estimated as

$\sim 1.66 \times 10^{-6}$ N. Hence, the particles remain inside the droplet once picked up after impact. On the other hand, the force developed due to the magnetic effect alters with the concentration of particles and the distance from magnet to droplet. As the droplet gets nearer to the magnet, it gains acceleration because of the force created under the magnetic effect. Since the particles are located loosely on the hydrophobic surface and the magnet is located below the surface (70 mm below the surface) during the experiments, the force created between particle and magnet interface can be formulated in the frame of an earlier study.[35] Hence, the force created as a result of the magnetic field is:

$$F_m = \phi M_s \forall_p L \left[\frac{m_O H}{K_B T} \right] \frac{H}{S} \tag{4}$$

where ϕ represents the volumetric particle concentration, calculated as %wt $\frac{(n_p \forall \sigma_p)}{\forall_{pt}}$, where n_p is the number of lose particles in volume covered by loose particles, $\forall_p$ is the approximate volume of a single particle, and $\forall_{pt}$ is the total volume of the particle layer as if it covers the whole hydrophobic surface (using the photographic imaging technique, the value of ϕ is estimated as 0.62). M_s denotes the saturated magnetization per unit volume, H is the magnetic field strength, m_O stands for particle magnetic moment, K_B is the Boltzmann constant, T is temperature, S is the spacing from magnet to droplet, and $L\left[\frac{m_O H}{K_B T}\right]$ is the Langevin function. The Langevin function becomes equal to unity (approximately) due to the large value of the term $\left(\left[\frac{m_O H}{K_B T}\right] = 10^4\right)$, since $L\left[\frac{m_O H}{K_B T}\right] = \coth\left(\frac{m_O H}{K_B T}\right) - \frac{1}{\left[\frac{m_O H}{K_B T}\right]}$. Utilizing specific values such as $\rho_c = 5170.4$ kg m^{-3} for particles, $\rho_w = 1000$ kg m^{-3} for water, $M_s = 6.6 \times 10^{-3}$ mT for the particles, and 0.005 wt% for concentration,[25] magnetic field strength (H) is $\sim 6.95 \times 10^4$ A m^{-1}, $S = 20$ mm of spacing from magnet to droplet outer surface, and small droplet volume (20 µL), magnetic force is calculated to be $\sim 2.3 \times 10^5$ N. When the droplet becomes close to the magnet, this force increases significantly due to the reduced distance (S) in eqn (4). Assuming the droplet impact height (s) equals the diameter of the droplet (4.67 mm) before the impact, magnetic field strength becomes $H \sim 7.24 \times 10^4$ A m^{-1}, resulting in a force influencing the particles of $\sim 6.8 \times 10^{-5}$ N.

Droplet behavior after impact

Water droplets impacted on loosely distributed ferroparticles over a hydrophobic surface with and without a magnetic field. Fig. 4 shows high-speed camera images for time frames with and without particles on the impacting substrate. The images also include the case where a magnetic field was applied. The spreading droplet liquid wets the non-functionalized ferroparticle surface and upon impact some particles are captured by the droplet fluid. This results in a change of the contact angle of the droplet because of the presence of particles in the droplet fluid, which lowers the contact angle almost $\sim 2°$–$4°$.[5] As the magnetic field is applied, the particles picked up by the droplet can further influence the surface tension and the contact angle. The surface tension because of the magnetic field can be formulated in accordance with earlier work.[36] After considering that the shape of the droplet resembles an ellipse, the surface tension yields:[36]

$$\gamma_m = \gamma\left\{\frac{16\chi}{3(1+\chi N)}\text{Bo}_M + \frac{s}{2}\right\} \qquad (5)$$

where χ represents initial magnetic susceptibility, N corresponds to demagnetizing, Bo_M is the magnetic bond number ($= \frac{F_{\text{Magnetic}}}{F_{\text{Surf-tension}}} = \frac{r_d \mu_o H^2}{\gamma}$, where r_d is droplet radius, μ_o is

magnetic permeability of free space, H is magnetic field strength), and s is the surface area parameter ($s = \frac{\sin^{-1}r}{r} + p$, where $r = \sqrt{1 - \frac{b_0^2}{a_0^2}}$ is the eccentricity, $p = \frac{b_0}{a_0}$ represents the aspect ratio of the droplet, and a_0, b_0 are major and minor axes of the droplet). Introducing the data presented in earlier work[29] ($\chi = 1.2$,[37] $N = 0.5$,[38]) and using the optical images for the droplet and assuming that the droplet resembles an elliptic shape, $\frac{b_0}{a_0}$ becomes 0.7 and B_{OM} yields a value $\text{Bo}_M \sim 0.1$ (because of low concentration of particles inside droplet), and eqn (5) results in $\frac{\gamma_m}{\gamma} = 1.025$. The small change in droplet geometry because of the magnetic field effect and observed from the optical images is due to the small change of the surface tension.

Fig. 5a shows droplet contact time with Weber number while Fig. 5b demonstrates the variation of spreading factor for the different cases considered in experiments. Contact time is related to end of droplet expansion and retraction periods prior to droplet rebound on the surface. The droplet contact time and spreading factor differ considerably in cases with and without loose particles on the surface and the presence or absence of a magnetic field. This variation associated with droplet expansion and retraction cycles on the surface is such that (i) the presence of ferroparticles in droplet liquid, due to them being picked up, increases surface tension while enhancing droplet adhesion on the surface due to increased surface tension force, (ii) shear stress on the impacted surface increases because of loosely distributed particles on the surface, and (iii) the mass of the droplet increases as a result of picking up particles while contributing to the kinetic energy loss during expansion and retraction. In the case involving the magnetic field, the force created on particles due to the magnetic field contributes significantly to kinetic energy loss during expansion and contraction cycles on the hydrophobic surface. This is reflected in Fig. 5a, where contact time remains lowest for all Weber numbers for the case where the magnetic field is applied. In general, contact time reduces as Weber number increases, which is mainly because of the energy dissipation on the surface in terms of friction, air drag, and work done during expansion as well as the work done against the pinning forces of particles particularly under the magnetic effect during expansion and contraction cycles. Functionalizing the ferroparticles towards reducing surface energy, *via* the dip-coating process, slightly improves the contact time. This is because of (i) small surface tension force between liquid and particle and (ii) interfacial tension to pick up particles by liquid inside the droplet is less likely, *i.e.* particles attach to the droplet surface rather than mixing with liquid, which can be seen in Fig. 4. Moreover, the shear force (F_s) at the droplet–substrate interface can be approximated by $F_s = \int_0^{R_d} \mu \frac{du_d(r)}{dn} 2\pi r dr$, where μ is viscosity, u_d is liquid velocity, r is variable along the radius, n is the space variable normal to the surface, and R_d is the wetted radius. The wetted area on the impacted surface can be simplified and
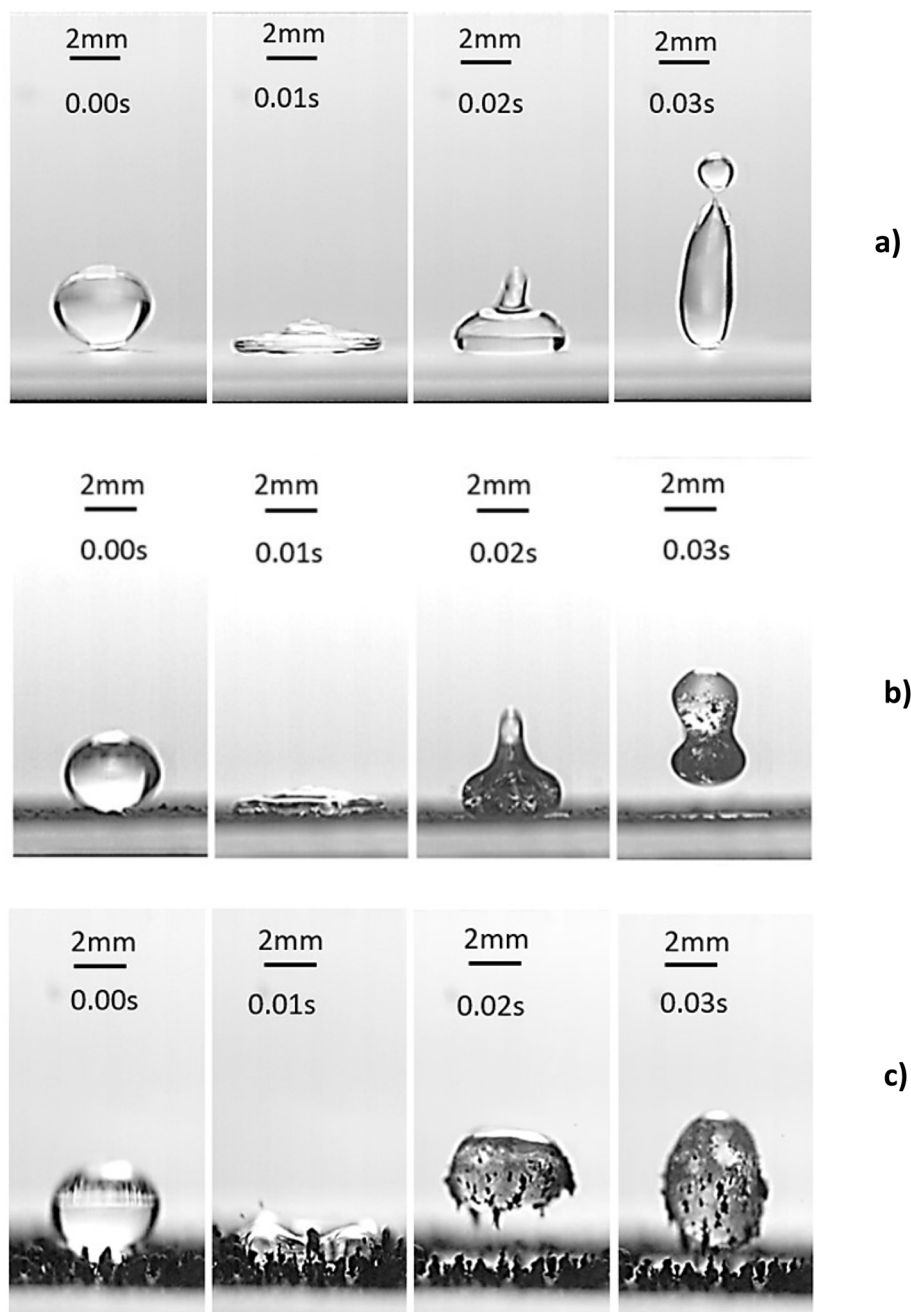
Fig. 4 High-speed camera images: (a) a droplet impacting on the hydrophobic surface, (b) a droplet impacting on the hydrophobic surface with loosely dispersed ferroparticles, and (c) a droplet impacting on the hydrophobic surface with loosely dispersed functionalized ferroparticles.

assumed to resemble a circle on the surface at the end of spreading, which is $\sim 1.26 \times 10^{-7}$ m^2, and average fluid velocity (assumed to be the same as spreading velocity) is 0.0024 m s^{-1}. This results in a maximum shear force of about 6.14×10^{-7} N at the end of the spreading. However, the droplet interfacial force, which is estimated as $\sim 1.47 \times 10^{-4}$ N, becomes larger than the estimated shear force. Therefore, shear force has a small effect on contact time as compared to interfacial adhesion force due to surface tension. It is worth mentioning that the interfacial force contributes to the droplet pinning while lowering the contact time of the droplet during expansion and retraction

cycles. In the case of spreading factor ($d_{\mathrm{m}}/d_{\mathrm{o}}$, where d_{m} is the maximum droplet spreading diameter on the surface and d_{o} is the droplet diameter prior to impact), as shown in Fig. 5b, the impacting droplet extends on the surface while the clustered particles maintain their locations over the surface because of the magnetic force created, i.e. due to the small thickness of the hydrophobized substrate (~ 0.2 mm), and magnetic force remains high. This gives rise to minimum droplet spreading over the impacted surface.

Fig. 6a demonstrates the restitution coefficient for various conditions, including with synthesized particles and in the
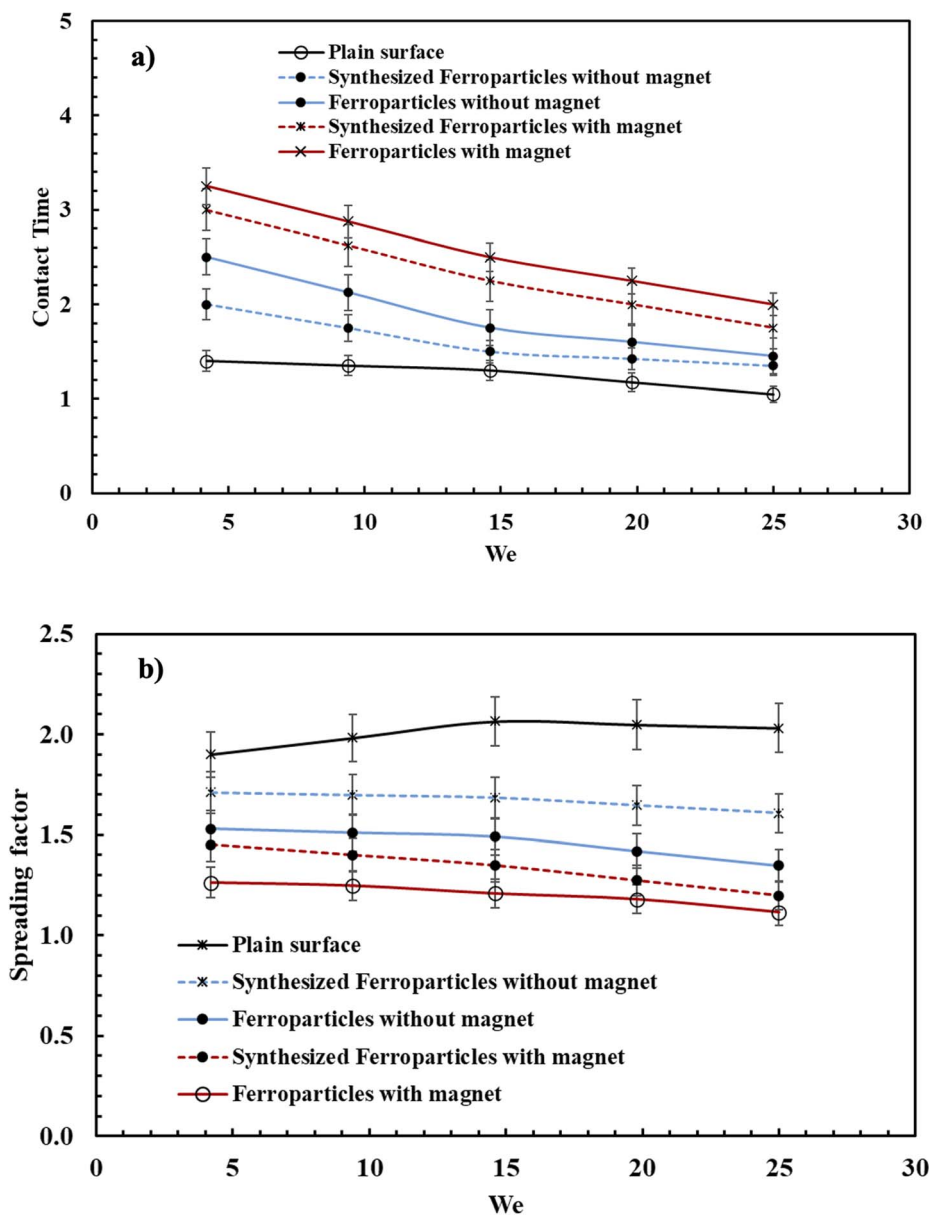
Fig. 5 (a) Contact time *vs.* Weber number for the different cases considered in the present study. (b) Spreading factor *vs.* Weber number for the different cases considered in the present study.

presence of the magnetic field. The restitution coefficient represents the ratio of velocity change prior to and after impact on the surface, *i.e.* $e = \dfrac{V_{d-s} - V_{d-f}}{V_{d-m} - V_{d-i}}$, where V_{d-m} is the droplet velocity at onset of impact, V_{d-i} is the initial velocity before fall from the stand-off condition ($V_{d-i} = 0$), V_{d-s} is impacted droplet velocity on the surface (varies during contact time), and V_{d-f} is the final droplet velocity on the surface ($V_{d-f} = 0$). It can also be written as $e \sim \sqrt{\dfrac{h_f}{h_i}}$, where h_f is droplet rebound height and h_i is droplet stand-off height. The Weber number represents the surface tension force over the inertia force of droplet, *i.e.* $\dfrac{\rho V_d^2 D_d}{\gamma}$, where ρ is density, V_d is velocity of the

droplet (depending on stand-off height), and D_d is the droplet equivalent diameter, which corresponds to the diameter of a perfectly spherical droplet having the same volume as the stand-off droplet. Similar to that of droplet contact time as shown in Fig. 4a, increasing the Weber number lowers the restitution coefficient. Force of inertia attains high values as the stand-off height increases. The droplet loses its kinetic energy upon impact and this loss is significant as the stand-off height becomes large. The presence of particles on the impacted surface contributes to kinetic energy loss, which increases as the magnetic field is introduced. However, functionalizing the particles causes less kinetic energy loss as compared to that corresponding to as-received particles. In this case, interfacial force ($\sim 1.56 \times 10^{-4}$ N) contributes to pinning of the droplet on
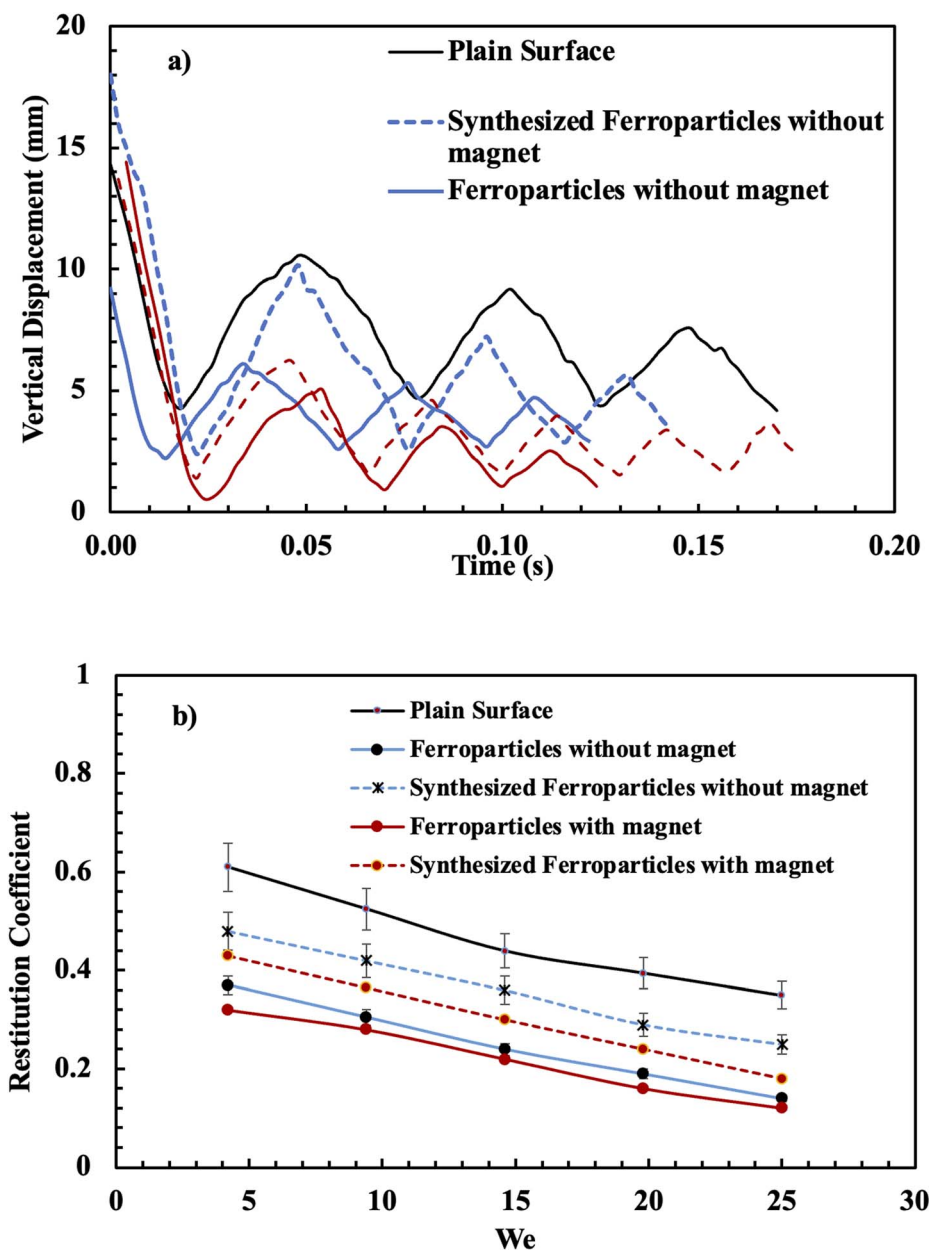
Fig. 6 (a) Rebound height *vs.* Weber number for the different cases considered in the present study. (b) Restitution coefficient *vs.* Weber number for the different cases considered in the present study.

the surface and shear force ($\sim 6.12 \times 10^{-7}$ N) contributes to kinetic energy loss after impact. The restitution coefficient reduces almost linearly with Weber number and the percentage reduction becomes similar for the cases considered. Fig. 6b shows rebound height with Weber number for all cases considered. Rebound height is influenced by the particles, which becomes more significant for the case with ferroparticles and magnetic field, *i.e.* in such a situation, the magnetic force created on particles contributes to pining of the droplet on the surface, which in turn causes droplet kinetic energy loss and attainment of low rebound height. It is worth mentioning that the maximum shear and interfacial forces are estimated as $\sim 6.14 \times 10^{-7}$ N and $\sim 1.56 \times 10^{-4}$ N, respectively. However, the

magnetic force is estimated as $\sim 6.8 \times 10^{-5}$ N for a magnetic field strength of $H \sim 7.24 \times 10^{4}$ A m^{-1}. These forces act in opposition to droplet inertial force for rebounding while contributing to low rebound height under the influence of the magnetic field. In the case of functionalized particles, the particles are not wetted by the droplet fluid, due to negative spreading rate,[39] and they are rather attached to the droplet surface during the rebounding cycle, which can be observed from Fig. 4. However, the force acting on particles, under the influence of the magnetic field, contributes to kinetic energy loss and the rebound height remains small, provided that droplet rebound height for as-received particles is less than that for functionalized particles. As-received particles are picked up

by the liquid upon impact; however, functionalized particles mainly attach to the droplet surface (Fig. 4). Fig. 6b demonstrates rebound height for the different configurations used in the experiments. Since droplet vertical position is associated with restitution coefficient in terms of $e \sim \sqrt{\dfrac{h_f}{h_i}}$, large restitution coefficients result in large rebound height. The droplet undergoes multiple rebounds after impact and because of energy dissipation, the peak rebound height decreases with the number of rebounds. This becomes visible for the case of as-received particles. Energy dissipation between peak heights is relatively larger for surfaces with particles than plain surfaces. This shows that interfacial resistance between particles and liquid, and shear resistance created at the surface increase with the presence of particles. Consequently, total energy dissipation before multiple rebounds increases. In addition, loosely distributed particles on the hydrophobic surface influence the wetting state of the substrate while lowering the droplet contact angle and increasing contact angle hysteresis. This causes an increased surface tension force during droplet expansion over the surface after impact through which dissipated energy increases during droplet expansion. For synthesized particles, droplet hysteresis remains low, and work done overcoming the surface tension becomes less during droplet spreading. This gives rise to higher peaks for the rebound height than those for the as-received particles case. In the case of an applied magnetic field, particles are pinned on the substrate surface creating a topology that modifies the surface wetting angle. In addition, some particles can be taken up by the droplet liquid (Fig. 3) while contributing to droplet pinning on the surface. Therefore, increased work done overcoming the surface tension force, due to high hysteresis, and the pinning effect of the magnetic force result in large energy dissipation causing low rebound height peaks. This is more pronounced for the other peaks of the rebound height.

Conclusions

An impacting droplet on a hydrophobic surface with loosely dispersed ferroparticles with and without a magnetic field is investigated. Dynamic analysis of the impacting droplet is conducted, in which spreading, retraction, and contact time on the surface are evaluated, and droplet rebound height is determined. To assess the energy dissipation of droplets after impact, experiments are repeated after incorporating synthesized particles to lower the hysteresis of the wetting angle at the surface. The surface is hydrophobized *via* the deposition of synthesized silica nanoparticles *via* the dip-coating technique. A high-speed camera system was utilized to record the impacting droplet motion. We demonstrated that the presence of loosely dispersed ferroparticles slightly alters the surface wetting state in terms of a slightly reduced contact angle (almost 2.5% reduction) and increased contact angle hysteresis (almost 5% increase), which becomes important in the presence of a magnetic force. However, the contact angle increases when the ferroparticles are functionalized to lower their surface free energy. Impacting droplet properties are influenced by the

loosely dispersed particles after impact. Some particles are picked up by the droplet liquid after impact, which is related to the positive spreading coefficient of the droplet liquid on particles, *i.e.* the liquid wets the particles. Because of high interfacial force between particles and the liquid ($\sim 1.56 \times 10^{-4}$ N), these particles remain inside the droplet during multiple rebounds. Droplet energy dissipation during impact increases due to the presence of particles while reducing the contact time at the surface, which becomes more visible at high Weber numbers. Droplet energy dissipation is related to (i) work done against surface tension force, due to reduced contact angle and increased contact angle hysteresis, during expansion and contraction, (ii) enhanced shear stress at the droplet bottom due to the presence of particles in the droplet bottom increasing the rate of fluid strain, and (iii) slightly increased droplet mass *via* particles being picked up by the droplet fluid upon impact. This becomes more apparent as the magnetic field is introduced. The particles are magnetically attached to the substrate surface, creating a surface topology that enhances the contact angle hysteresis. In addition, only a few particles can be picked up by droplet liquid after impact because of the magnetic force ($\sim 2.3 \times 10^{-5}$ N), which is higher than the capillary force ($\sim 2.69 \times 10^{-6}$ N). Restitution coefficient and rebound height are reduced by the particles, which becomes significant as the magnetic field is introduced. The reduction of restitution coefficient and rebound height reaches about 40% and above due to the magnetic field. Functionalized particles attach to the droplet surface rather than being picked up by the droplet fluid because of the negative spreading coefficient. Since the interfacial force ($\sim 1.56 \times 10^{-4}$ N) is bigger than the magnetic force acting on the particles ($\sim 2.3 \times 10^{-5}$ N), no new droplet or particle separation is observed after the second rebound. The present study provides a detailed analysis of impacting droplets on hydrophobic surfaces with dispersed loose particles and provides useful information on impacting droplet mobility and characteristics under the influence of a magnetic field.

Author contributions

B. S. Yilbas did the research work with the collaboration of other co-authors and wrote the manuscript. Ghassan Hassan did experimental and analytical work and contributed to the writing of the manuscript. H. Al-Qahtani did part of the experimental and analytical work and contributed to the writing of the manuscript. A. Al-Sharafi did part of the experimental work and contributed to the writing of the manuscript.

Conflicts of interest

The authors declare that there is no conflicts of interest.

Data availability

No primary research results, software or code have been included and no new data were generated or analysed as part of this review.

Acknowledgements

References

1 L. Junhui and P. B. Weisensee, Low Weber number droplet impact on heated hydrophobic surfaces, *Exp. Therm. Fluid Sci.*, 2022, **130**, 110503, DOI: **10.1016/j.expthermflusci.2021.110503**.

2 D. Liu, M. Sun, J. Zhang, R. Hu, W. Fu, T. Xuanyuan and W. Liu, Single-cell droplet microfluidics for biomedical applications, *Analyst*, 2022, **147**, 2294–2316, DOI: **10.1039/d1an02321g**.

3 W. L. Ng, X. Huang, V. Shkolnikov, G. L. Goh, R. Suntornnond and W. Y. Yeong, Controlling droplet impact velocity and droplet volume: key factors to achieving high cell viability in sub-nanoliter droplet-based bioprinting, *Int. J. Bioprint.*, 2021, **8**, 424, DOI: **10.18063/ijb.v8i1.424**.

4 B. S. Yilbas, A. A. Abubakar, H. Ali, A. Al-Sharafi, A. Z. Sahin, M. Sunar and H. Al-Qahtani, Impacting water droplets can alleviate dust from slanted hydrophobic surfaces, *Langmuir*, 2021, **37**(14), 4355–4369, DOI: **10.1021/acs.langmuir.1c00436**.

5 B. S. Yilbas, A. A. Abubakar, G. Hassan, H. Al-Qahtani, A. Al-Sharafi, A. Z. Alzahrani and A. S. Mohammed, Ferro-fluid droplet impact on hydrophobic surface under magnetic influence, *Surf. Interfaces*, 2022, **29**, 101731, DOI: **10.1016/j.surfin.2022.101731**.

6 A. F. Demirörs, S. Aykut, S. Ganzeboom, Y. A. Meier and E. Poloni, Programmable droplet manipulation and wetting with soft magnetic carpets, *Appl. Phys. Sci.*, 2021, **118**, 46, DOI: **10.1073/pnas.2111291118**.

7 G.-P. Zhu, Q.-Y. Wang, Z.-K. Ma, S.-H. Wu and Y.-P. Guo, Droplet manipulation under a magnetic field: a review, *Biosensors*, 2022, **12**, 156, DOI: **10.3390/bios12030156**.

8 R. N. Wenzel, Resistance of solid surfaces to wetting by water, *Ind. Eng. Chem.*, 1936, **28**, 988–994.

9 A. B. D. Cassie and S. Baxter, Wettability of porous surfaces, *Trans. Faraday Soc.*, 1944, **40**, 546–551.

10 X. Liu, Y. Zhang and X. Chen, The impact and spreading of a droplet on a hydrophobic surface: The role of surface roughness and droplet size, *J. Fluid Mech.*, 2016, **804**, 60–78.

11 P. Emerson, J. Crockett and D. Maynes, Thermal atomization during droplet impingement on superhydrophobic surfaces: Influence of Weber number and micropost array configuration, *Int. J. Heat Mass Transfer*, 2021, **164**, 120559, DOI: **10.1016/j.ijheatmasstransfer.2020.120559**.

12 C. Clanet, C. Béguin, D. Richard and D. Quéré, Maximal deformation of an impacting drop, *J. Fluid Mech.*, 2004, **517**, 199–208, DOI: **10.1017/S0022112004000904**.

13 I. S. Bayer and C. M. Megaridis, Contact angle dynamics in droplets impacting on flat surfaces with different wetting characteristics, *J. Fluid Mech.*, 2006, **558**, 415–449, DOI: **10.1017/S0022112006000231**.

14 J. M. Gordillo, G. Riboux and E. S. Quintero, A theory on the spreading of impacting droplets, *J. Fluid Mech.*, 2019, **866**, 298–315, DOI: **10.1017/jfm.2019.117**.

15 Y. Yonemoto and T. Kunugi, Analytical consideration of liquid droplet impingement on solid surfaces, *Sci. Rep.*, 2017, **7**, 2362, DOI: **10.1038/s41598-017-02450-4**.

16 M. Wörner, Maximum spreading of an impacting drop, *Int. J. Multiphase Flow*, 2023, **167**, 104528.

17 A. Marmur, The lotus effect: Superhydrophobicity and metastability, *Langmuir*, 2004, **20**, 3517–3519.

18 B. S. Yilbas, A. A. Abubakar, G. Hassan, H. Al-Qahtani, A. Al-Sharafi, A. A. Alzahrani and A. S. Mohammed, Ferro-fluid droplet impact on hydrophobic surface under magnetic influence, *Surf. Interfaces*, 2022, **29**, 101731, DOI: **10.1016/j.surfin.2022.101731**.

19 A. Naga, A. Kaltbeitzel, W. S. Y. Wong, L. Hauer, H.-J. Butt and Do. Vollmer, How a water drop removes a particle from a hydrophobic surface, *Soft Matter*, 2021, **17**, 1746–1755, DOI: **10.1039/D0SM01925A**.

20 C.-H. Hsu, Y.-H. Chiu, F.-T. Tsai, S.-H. Chou and L.-T. Sheng, The effects of magnetic field control on the aggregation of magnetic particles on the heating surface during pool boiling, *Int. Commun. Heat Mass Transfer*, 2024, **152**, 107289, DOI: **10.1016/j.icheatmasstransfer.2024.107289**.

21 Z. Huang, *et al.*, Dynamic behavior of a droplet impacting on a magnetic surface, *Appl. Surf. Sci.*, 2019, **473**, 111–118.

22 T. Kang, Y. You, R. Hoptowit, M. M. Wall and S. Jun, Effect of an oscillating magnetic field on the inhibition of ice nucleation and its application for supercooling preservation of fresh-cut mango slices, *J. Food Process Eng.*, 2021, **300**, 110541, DOI: **10.1016/j.jfoodeng.2021.110541**.

23 N.-T. Nguyen, K. M. Ng and X. Huang, Manipulation of ferrofluid droplets using planar coils, *Appl. Phys. Lett.*, 2006, **89**, 5, DOI: **10.1063/1.2335403**.

24 G. Hassan, B. S. Yilbas, A. A. Abubakar, A. Al-Shari and H. Al-Qahtani, A comparative study for ferro particles cloaking and wetting characteristics, *Sci. Rep.*, 2024, **14**, 16292, DOI: **10.1038/s41598-024-66944-8**.

25 A. A. Abubakar, B. S. Yilbas, H. Al-Qahtani and A. Alzaydi, Environmental dust repelling from hydrophilic/hydrophobic surfaces under sonic excitations, *Sci. Rep.*, 2020, **10**, 19348, DOI: **10.1038/s41598-020-76418-2**.

26 S. Bhattacharya, J. J. Charonko and P. P. Vlachos, Particle image velocimetry (PIV) uncertainty quantification using moment of correlation (MC) plane, *Meas. Sci. Technol.*, 2018, **29**, 115301.

27 G. Hassan, B. S. Yilbas, A. A. Abubakar, H. Al-Qahtani and A. Al-Sharafi, Dynamics of droplet motion over hydrophobic surfaces with functionalized and non-functionalized ferro particles, *RSC Adv.*, 2023, **13**, 34866–34875.

28 G. Hassan, B. S. Yilbas, A. Abdulhamid Abubakar, A. Al-Sharafi and H. Al-Qahtani, A comparative study for ferro

particles cloaking and wetting characteristics, *Sci. Rep.*, 2024, **14**, 16292.

29 G. Hassan, B. S. Yilbas, A. Abdulhamid Abubakar, A. Al-Sharafi and H. Al-Qahtani, A comparative study for ferro particles cloaking and wetting characteristics, *Sci. Rep.*, 2024, **14**, 16292.

30 B. S. Yilbas, G. Hassan, A. Al-Sharafi, H. Ali, N. Al-Aqeeli and A. Al-Sarkhi, Water droplet dynamics on a hydrophobic surface in relation to the self-cleaning of environmental dust, *Sci. Rep.*, 2018, **8**, 2984.

31 B. S. Yilbas, A. Abdulhamid Abubakar, G. Hassan, H. Al-Qahtani, A. Al-Sharafi, A. A. Alzahrani and A. S. Mohammed, Ferro-fluid droplet impact on hydrophobic surface under magnetic influence, *Surf. Interfaces*, 2022, **29**, 101731.

32 F. Heib, W. M. Munief, S. Ingebrandt, R. Hempelmann and M. Schmitt, Influence of different chemical surface patterns on the dynamic wetting behaviour on flat and silanized silicon wafers during inclining-plate measurements: An experimental investigation with the high-precision drop shape analysis approach, *Colloids Surf., A*, 2016, **508**, 274–285.

33 A. M. Ali, N. Yahya and S. Qureshi, Interactions of ferro-nanoparticles (hematite and magnetite) with reservoir sandstone: implications for surface adsorption and interfacial tension reduction, *Pet. Sci.*, 2020, 1–19.

34 M. Shikida, K. Takayanagi, H. Honda, H. Ito and K. Sato, Development of an enzymatic reaction device using magnetic bead-cluster handling, *J. Micromech. Microeng.*, 2006, **16**, 1875.

35 K. Bai, J. Casara, A. Nair-Kanneganti, A. Wahl, F. Carle and E. Brown, Effective magnetic susceptibility of suspensions of ferromagnetic particles, *J. Appl. Phys.*, 2018, **124**, 123901.

36 A. Ahmed, B. A. Fleck and P. R. Waghmare, Maximum spreading of a ferrofluid droplet under the effect of magnetic field, *Phys. Fluids*, 2018, **30**(30), 77102.

37 K. Bai, J. Casara, A. Nair-Kanneganti, A. Wahl, F. Carle and E. Brown, Effective magnetic susceptibility of suspensions of ferromagnetic particles, *J. Appl. Phys.*, 2018, **124**, 12.

38 T. A. Franklin, Ferrofluid Flow Phenomena. PhD diss., Massachusetts Institute of Technology, *J. Franklin Inst.*, 2003.

39 O. Arjmandi-Tash, N. M. Kovalchuk, A. Trybala, I. V. Kuchin and V. Starov, Kinetics of Wetting and Spreading of Droplets over Various Substrates, *Langmuir*, 2017, **33**(18), 4367–4385, DOI: **10.1021/acs.langmuir.6b04094**.